Antiferromagnetic correlations and impurity broadening of NMR linewidths in cuprate superconductors

J. W. Harter,[1] B. M. Andersen,[1,2] J. Bobroff,[3] M. Gabay,[3] and P. J. Hirschfeld[1,3]
[1]*Department of Physics, University of Florida, P.O. Box 118440, Gainesville, Florida 32611, USA*
[2]*Laboratoire de Physique Quantique, ESPCI, 10 Rue de Vauquelin, 75231 Paris, France*
[3]*Laboratoire de Physique des Solides, Université Paris-Sud, 91405 Orsay, France*
(Received 27 September 2006; published 23 February 2007)

We study a model of a *d*-wave superconductor with strong potential scatterers in the presence of antiferromagnetic correlations and apply it to experimental nuclear magnetic resonance (NMR) results on Zn impurities in the superconducting state of $YBa_2Cu_3O_{7-\delta}$. We then focus on the contribution of impurity-induced paramagnetic moments, with Hubbard correlations in the host system accounted for in Hartree approximation. We show that local magnetism around individual impurities broadens the line, but quasiparticle interference between impurity states plays an important role in smearing out impurity satellite peaks. The model, together with estimates of vortex lattice effects, provides a semiquantitative description of the impurity concentration dependence of the NMR line shape in the superconducting state, and gives a qualitative description of the temperature dependence of the line asymmetry. We argue that impurity-induced paramagnetism and resonant local density of states effects are both necessary to explain existing experiments.

DOI: 10.1103/PhysRevB.75.054520 PACS number(s): 74.25.Ha, 74.72.Bk, 74.81.−g

I. INTRODUCTION

The response of a correlated electron system to a local perturbation can often provide important information about the ground state of the pure system. This principle has been successfully applied to the substitution of various impurities, particularly Zn, Ni, and Li for Cu in the CuO_2 planes of various high-T_c superconductors, particularly in $YBa_2Cu_3O_{7-\delta}$.

In addition to traditional studies of the effect of impurities on bulk properties, local probes such as NMR and scanning tunneling spectroscopy (STS) have provided considerable information about how electronic wave functions are distorted near the impurity site. In the normal state of this system, NMR has shown that impurities enhance local antiferromagnetic correlations,[1,2] and in the presence of the applied dc field, then display a staggered pattern of magnetization, which decays over a few lattice spacings. This polarizability $\delta\chi$ has, moreover, a characteristic temperature dependence, which is Curie-like $\delta\chi \sim T^{-1}$ in the underdoped system, but evolves to Curie-Weiss-like behavior $\delta\chi \sim (T+\theta)^{-1}$ in the optimal to overdoped range.[3] Because θ increases rapidly with doping, it has sometimes been interpreted as a Kondo temperature, enhanced in the presence of higher carrier densities capable of screening the magnetic moment induced by the impurity. Other pictures of this phenomenon, which do not rely on Kondo screening, have been put forward as well. For example, in the weak-coupling approaches of Bulut[4,5] and Ohashi,[6] an extended potential is found to produce a Curie-Weiss-like local susceptibility in a Hubbard model treated in mean field, due to the coupling of the antiferromagnetic $\mathbf{q}=(\pi,\pi)$ response of the lattice system to the uniform $\mathbf{q}=0$ response by the inhomogeneity.

In the superconducting state, interpretation of the NMR signal is complicated by the intrinsic field distribution introduced by the vortex lattice, and by the vanishing of the $\mathbf{q}=0$ susceptibility in the singlet pair state. On the other hand, Ohashi[7] argued that the mode-coupling effect induced by the inhomogeneity persists and is relatively enhanced by the opening of the gap. Experimentally, the enhancement of the local susceptibility was indeed found below T_c,[8] and tended to become a large constant value at very low T. Recently, Ouazi *et al.*[9] measured the evolution of the ^{17}O NMR line with increasing Zn concentration and observed the formation of the staggered polarization cloud in the superconducting state. They argued that the primary line shift was due to the nearly field-independent vortex distribution and that the broadening was a combination of the enhanced impurity effect and the simultaneous narrowing of the vortex field distribution due to the increased penetration depths λ in the dirtier systems. Missing from this picture is an understanding of the magnitude of the impurity broadening and how it really occurs; if one considers only a single impurity, one expects large values of the magnetization on the Zn nearest-neighbor sites, which should lead to a well-defined satellite line, as in the case of NMR on Li impurities in the normal state.[3] These have not been detected in samples with Zn concentrations at the percent level.

An alternate picture of the observed phenomena in the superconducting state is obtained if one considers the local susceptibility due to quasiparticles in the *d*-wave superconductor, proportional to the local density of quasiparticle states (LDOS) at the Fermi level. A significant enhancement of the local susceptibility is then to be expected from quasiparticle bound states alone. Williams *et al.*[10] proposed that these quasiparticle resonant states—corresponding to those imaged by scanning tunneling microscopy (STM) experiments around Zn atoms in $Bi_2Sr_2CaCu_2O_{8+x}$ (BSCCO-2212) (Ref. 11)—might be entirely responsible for the enhanced magnetic response near Zn seen in NMR. Chang *et al.*[12] then argued that for a single nonmagnetic impurity, the temperature dependence of the observed spin-lattice relaxation time and Knight shift could indeed be qualitatively understood in terms of LDOS enhancement due to impurity bound states alone.

There are some difficulties with the naive interpretation of the NMR measurements entirely in terms of the LDOS enhancement near impurities, however. First, significant T-dependent enhancements of local susceptibilities near nonmagnetic impurities occur in the normal state of optimally doped cuprates as well. An "LDOS-only" approach cannot account for this since impurities do not produce LDOS resonances in the normal (metallic) state. Second, the NMR experiments on these materials clearly show that the magnetization near a Zn site alternates in sign. This is incompatible with the paramagnetic character of the quasiparticle Pauli susceptibility, i.e., the susceptibility enhancement due to impurity bound states is always positive, so while Friedel-type oscillations can occur, the magnetization is always aligned with the external field. Finally, the "Knight shift" calculated in Ref. 12 is defined as a local susceptibility enhancement very near the impurity; in fact, the measured Knight shift in experiments where the nucleus is distinct from the impurity itself is the shift of the *total* NMR line, determined by sites far from the impurities.

Thus, a theoretical calculation which includes local magnetic moment formation, together with quasiparticle impurity bound states and their interference, is of considerable interest in the understanding of the simple but striking features of the NMR experiments in the superconducting state.[8,9] A complete theory of these phenomena must be able to account not only for the Knight shift but also for the detailed behavior of the site-specific NMR lines produced by the different nuclei probed in different experiments. In this paper, we study Zn ions modeled as strong potential scatterers in a d-wave superconductor with antiferromagnetic (AF) correlations treated within a weak-coupling approach, as in Ref. 7. In Sec. II, we describe the model for a single impurity in a d-wave superconductor with correlations and the magnetization it induces, then in Sec. III, we study interference effects on the magnetization distribution when many impurities are present. In Sec. IV, we combine the predicted impurity contribution to the NMR linewidths with vortex effects, and compare it to the ^{17}O NMR experiment of Ouazi *et al.*[9] Section V is devoted to the application of the same results to compare with experiments using the ^{7}Li nucleus. In Sec. VI, we present our conclusions and implications for other experiments on the cuprates, as well as new questions raised by our interpretation.

II. SINGLE IMPURITY IN SYSTEM WITH ANTIFERROMAGNETIC CORRELATIONS

A. Formalism

A strong nonmagnetic impurity in the presence of antiferromagnetic correlations will induce a pattern of local staggered magnetization with maximum peaks on nearest-neighbor sites. When many impurities are present, these local states interfere, washing out nearest-neighbor peaks and producing a smooth distribution of local fields. The NMR line shift and broadening are caused by this impurity effect in conjunction with the vortex contribution. In order to study this magnetic behavior, we begin with a two-dimensional tight-binding Hamiltonian of a d-wave superconductor with AF correlations treated within mean-field theory,

$$\hat{H} = -\sum_{ij\sigma} t_{ij}\hat{c}^{\dagger}_{i\sigma}\hat{c}_{j\sigma} + \sum_{i\sigma}(Un_{i-\sigma} + \epsilon_{i\sigma} - \mu)\hat{c}^{\dagger}_{i\sigma}\hat{c}_{i\sigma} + \sum_{i\delta}(\Delta_{\delta i}\hat{c}^{\dagger}_{i\uparrow}\hat{c}^{\dagger}_{i+\delta\downarrow} + \text{H.c.}), \tag{1}$$

where the hopping term includes nearest-neighbor hopping t and next-nearest-neighbor hopping t', $\epsilon_{i\sigma} \equiv V_{\text{imp}} - g\mu_B \frac{1}{2} B\sigma$ describes the impurity and Zeeman site energies, μ is the chemical potential, $\Delta_{\delta i}$ is the nearest neighbor pairing potential, and $\delta \in \{\hat{\mathbf{x}}, -\hat{\mathbf{x}}, \hat{\mathbf{y}}, -\hat{\mathbf{y}}\}$ are unit lattice vectors to nearest neighbors. Here, $g \approx 2$ is the electron g factor, μ_B is the Bohr magneton, and B is the applied field along the c axis. The electron number and d-wave (singlet) pairing parameters are defined as $n_{i\sigma} = \langle \hat{c}^{\dagger}_{i\sigma}\hat{c}_{i\sigma}\rangle$ and $\Delta_{\delta i} = V\langle \hat{c}_{i\uparrow}\hat{c}_{i+\delta\downarrow} + \hat{c}_{i+\delta\uparrow}\hat{c}_{i\downarrow}\rangle/2$. We note that the Hamiltonian [Eq. (1)] has been used extensively to study bulk competing phases, disorder, and vortex-induced magnetization, as well as novel bound states at interfaces between antiferromagnets and superconductors.[13]

Equation (1) can be diagonalized by using the Bogoliubov transformation. The corresponding Bogoliubov–de Gennes equations must be solved iteratively until a self-consistent solution is found,

$$\begin{pmatrix} \hat{\xi}_{\uparrow} & \hat{\Delta} \\ \hat{\Delta}^{*} & -\hat{\xi}^{*}_{\downarrow} \end{pmatrix} \begin{pmatrix} u_n \\ v_n \end{pmatrix} = E_n \begin{pmatrix} u_n \\ v_n \end{pmatrix}, \tag{2}$$

where positive eigenvalues correspond to spin-up excitations and negative eigenvalues correspond to spin-down excitations. The matrix operators are defined by $\hat{\xi}_{\sigma}u_{n,i} = -\Sigma_{ij}t_{ij}u_{n,j} + (Un_{i-\sigma} + \epsilon_{i\sigma} - \mu)u_{n,i}$ and $\hat{\Delta}u_{n,i} = \Sigma_{\delta}\Delta_{\delta i}u_{n,i+\delta}$. The mean-field parameters, updated after each iteration until sufficient convergence is achieved, can be computed by

$$\Delta_{\delta i} = \frac{V}{4}\sum_{n}(u_{n,i}v^{*}_{n,i+\delta} + u_{n,i+\delta}v^{*}_{n,i})\tanh\left(\frac{E_n}{2T}\right), \tag{3}$$

and $n_{i\sigma} = (n_i + \sigma m_i)/2$, where n_i is the average electron density at site i and m_i is the magnetization on site i,

$$n_i = 1 - \frac{1}{2}\sum_{n}(|u_{n,i}|^2 - |v_{n,i}|^2)\tanh\left(\frac{E_n}{2T}\right), \tag{4}$$

$$m_i = -\frac{1}{2}\sum_{n}(|u_{n,i}|^2 + |v_{n,i}|^2)\tanh\left(\frac{E_n}{2T}\right). \tag{5}$$

It is important to note that in this model the superconducting pairing is taken to be a phenomenological constant and is not affected by the Hubbard repulsion U. In this sense, results may differ from true inhomogeneous spin-fluctuation models, where both magnetism and pairing are driven by the same correlations.

When deciding which ordered phase is the ground state, it is necessary to know the total energy E of the system, defined as $\langle \hat{H} \rangle$. It is given by

$$E = \mathrm{KE} + \sum_i \left[\epsilon_{i\uparrow} \frac{n_i + m_i}{2} + \epsilon_{i\downarrow} \frac{n_i - m_i}{2} - \mu n_i + \frac{U}{4}(n_i^2 - m_i^2) - \sum_\delta \frac{|\Delta_{\delta i}|^2}{V} \right], \quad (6)$$

where KE is the kinetic energy of the system,

$$\mathrm{KE} = -\frac{1}{2}\sum_{ijn} t_{ij}(v_{n,i}v_{n,j}^* - u_{n,j}u_{n,i}^*)\tanh\left(\frac{E_n}{2k_BT}\right). \quad (7)$$

We will often speak of the total magnetic moment (or spin) of the system. This is given (in units of $\hbar$) by

$$S_z = \frac{1}{2}\sum_i m_i. \quad (8)$$

We will also make reference to the d-wave order parameter, defined as

$$d_i = \frac{1}{4}(\Delta_{x,i} + \Delta_{-x,i} - \Delta_{y,i} - \Delta_{-y,i}). \quad (9)$$

In the following, we operate at a band filling $n=0.85$ such that the ground state of the homogeneous system is always pure d wave of the form $\Delta_{\mathbf{k}} \propto \cos k_x - \cos k_y$.

Finally, we have occasional need for spatially resolved spectral information and so also calculate the LDOS $N(E,i)$ via

$$N(E,i) = \frac{1}{2}\sum_n (|u_{n,i}|^2 \delta(E - E_n) + |v_{n,i}|^2 \delta(E + E_n)). \quad (10)$$

The chemical potential μ is adjusted to produce an average electron density of 0.85, corresponding to 15% hole doping characteristic of optimally doped cuprates. We give all energies in units of t and set $t' = -0.2$ to mimic typical Fermi surface shapes found in these systems and $V=1$ to give a critical temperature of 0.15, in units where $k_B=1$.

B. Single-impurity phase diagram

In Fig. 1, we give a schematic phase diagram for the model [Eq. (1)] with crude phase boundary lines and details suppressed for simplicity. Here, "AF," "F," and "P" denote self-consistent mean-field phases of Eq. (1), characterized roughly as antiferromagnetic, ferromagnetic, and paramagnetic, respectively. For example, within the AF region, it is well known that spin-density waves with ordering vectors other than exactly $\mathbf{Q}=(\pi,\pi)$ can be stabilized with details depending on the doping level and band-structure parameters. Since we have included a separate nearest-neighbor pairing interaction term V in the Hamiltonian in order to study the superconducting state, we have also indicated in Fig. 1 the regions of doping over which nearest-neighbor d- or s-wave pairing symmetry characterizes the ground state. Note that in this case the ordered magnetic phases coexist with superconductivity within the model; again, details have been suppressed for simplicity, and because we are here primarily concerned with the paramagnetic (d-wave superconducting) phase.

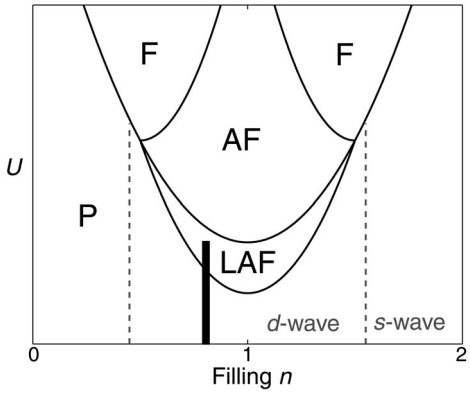

FIG. 1. $T=0$, U-n phase diagram for Hubbard plus nearest-neighbor pairing model treated in the mean field used in this work. F, AF, and P are the usual ferromagnetic, antiferromagnetic, and paramagnetic phases found for the homogeneous Hubbard model. LAF is the local antiferromagnetic phase where spontaneous staggered moments form around a single potential scatterer. The gray lines indicate the boundaries of coexistence of d- and s-wave superconductivities with the magnetic phases. Calculations are performed in the dark rectangle region between $0 < U < 2.0$ and at 15% hole doping, $n=0.85$.

Upon addition of a single strong impurity potential to the model, we find new inhomogeneous ground states present. Of most interest is a region of local staggered magnetism surrounding the impurity, referred to as the "local antiferromagnetic" (LAF) phase. In this phase, the impurity-induced staggered magnetization vanishes at a large distance from the impurity, and the net spin S_z summed over the whole system is found to be 1/2.[7] At larger U, the impurity still generates a net spin of 1/2, but the long-range ordering dominates, and the staggered magnetization has the maximum polarization arbitrarily far from the impurity. For a given fixed band structure and doping $n=0.85$, we have plotted the transition line between the (total) $S_z=0$ state and the $S_z=1/2$ state for varying U and impurity potential V_{imp}; clearly, increasing either U or V_{imp} tends to favor the local magnetic "spontaneous moment" state. In the lower panel of Fig. 2, we show the staggered magnetization patterns in each of the states for increasing U. Note that, in general, we do *not* find an intermediate state with $S_z=0$ *and* impurity-induced magnetism, in contrast to a recent study of the same Hamiltonian in Ref. 14, and we believe the presence of this state to be an artifact of the particular size system studied by these authors. We find generically either a $S_z=1/2$ state with local staggered magnetic order, or a state with no local magnetization at all in zero field, referred to as $S_z=0$ in Fig. 2. This is consistent with the results of Wang and Lee,[15] albeit derived in the weak coupling limit rather than for the t-J model. Similar results were obtained by Tsuchiura *et al.*[16]

We recover other single-impurity results known for this model, which we state for the sake of completeness. For example, the d-wave order parameter is strongly suppressed in the vicinity of a strong potential scatterer, mostly over a length scale of one lattice spacing but with a longer-range decay envelope over the coherence length ξ_0 (Fig. 3). The impurity also induces a much smaller s-symmetry order pa-

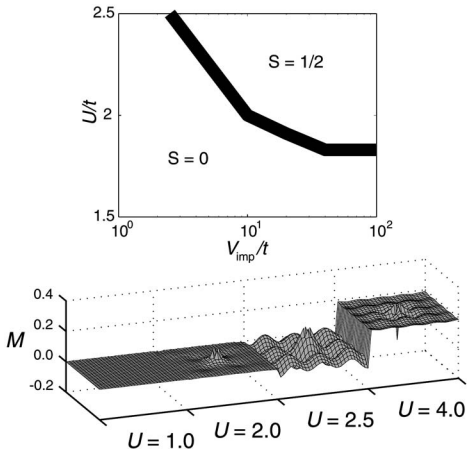

FIG. 2. Top: phase diagram for a single impurity as a function of the impurity potential V_{imp} and U, as determined by the presence of a nonzero magnetization at $T=0.013$. Note that there are only two phases, $S_z=0$ and $S_z=1/2$. Bottom: for strong impurity with $V_{\mathrm{imp}}=100$, dependence on U of the staggered magnetization, defined as $M_i=(-1)^i m_i$, for a 28×28 system. The system is completely nonmagnetic ($M=0$) for small values of U, assumes a local staggered state for intermediate values, and saturates toward a roughly homogeneous AF phase for large values. For the cases with nonzero magnetization, $S_z=1/2$. The wavelike AF ordering in the bulk for $U=2.5$ and 4.0 is due to finite-size effects and the periodic boundary conditions of the system.

rameter (not shown) and gives rise to a strong resonance in the LDOS near the Fermi level. The spatial intensity of the resonant state is centered primarily on the nearest-neighbor sites of the impurity (Fig. 4), in apparent conflict with the most naive interpretation of STM experiments; there are several competing explanations why this could be so. These phenomena have been reviewed and references given in Ref. 17 (see also Ref. 18).

C. Response of $S_z=0$ state to applied field

In this paper, we focus primarily on the impurity-induced state which has a net spin $S_z=0$ in zero field. This is because

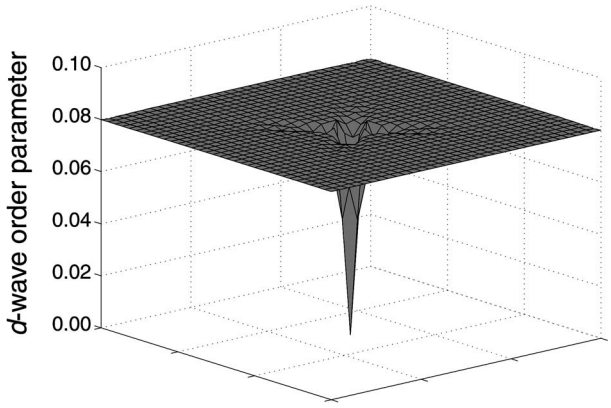

FIG. 3. d-wave order parameter suppression at an impurity of strength $V_{\mathrm{imp}}=100$ for $U=1.75$, $V=1$, 34×34 system, $g\mu_B B/2=0.004$, and $T=0.013$.

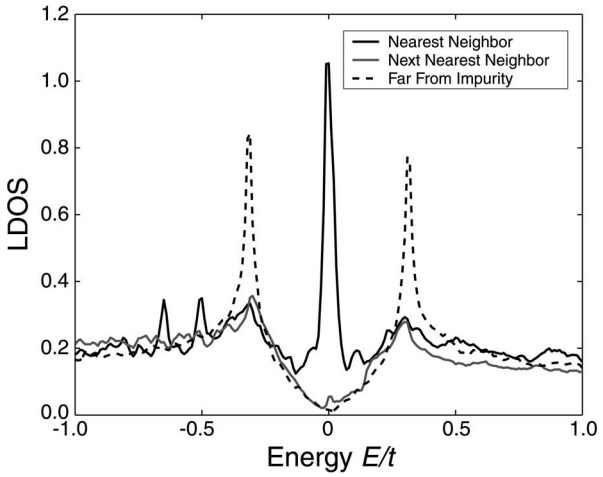

FIG. 4. The LDOS for a single-impurity system displaying paramagnetic behavior ($U=1.25$, $T=0.013$, and $g\mu_B B/2=0.004$), computed using a 28×28 system and 20×20 supercell. This result is in agreement with past studies using a similar model (Ref. 14).

there is no evidence for impurity-induced magnetization of any kind in zero field for almost all of the $YBa_2Cu_3O_{7-\delta}$ (YBCO) phase diagram.[19] NMR experiments, which are sometimes cited as providing evidence for spontaneous impurity-induced magnetization, are of necessity performed in finite applied field. Current $B=0$ neutron scattering[20] and muon spin resonance (μSR) (Ref. 21) measurements find no evidence of ordered static magnetization at any wave vector. Furthermore, both NMR and direct susceptibility measurements indicate that the induced states are paramagnetic, i.e., the magnetization vanishes proportional to the applied field. We note that there is considerable recent evidence that the situation is different in $La_{1-x}Sr_xCuO_4$ (LSCO), where static magnetism appears to exist even without an applied external field at low temperatures.[22,23] This may also explain unusual transport properties in LSCO compared to YBCO.[24,25]

With these considerations in mind, we choose a value of U, which will induce significant antiferromagnetic correlations close to half filling, but is not sufficient to cause the formation of magnetic moments around impurities in zero field. The impurity is taken to have an on-site spin-independent potential of strength $V_{\mathrm{imp}}=100$, roughly consistent with STM at least as far as the energy of the Zn LDOS resonance is concerned. To start, we study the Bogoliubov–de Gennes equations for a single such impurity with systems of the size of 34×34 with periodic boundary conditions. The Zeeman response of the electronic spins to the applied field is included in the $\epsilon_{i\sigma}$ term in Eq. (1), as discussed above. In our approach, we do not include the orbital response of the system to the applied vector potential, but rather we attempt to account for the presence of the vortex state phenomenologically (see below). We wish to compare our results with the data from the experiment of Ouazi *et al.*[9] we therefore take $t=100$ meV and set $|g\mu_B B/2|=0.004$ ($B\approx7$ T) and $T=0.013$ ($T\approx15$ K). Application of such a field induces, as expected,[4–7] a local staggered magnetization of the Cu spins around the impurity site, depicted in Fig. 5.

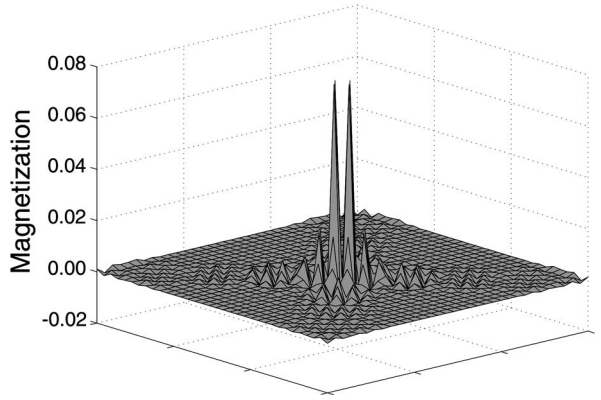

FIG. 5. The field-induced local magnetization for $U=1.75$, $g\mu_B B/2=0.004$, and $T=0.013$ on a 34×34 system. The total moment of the system is $\langle S_z\rangle=0.294$. Weak long-range AF correlations extend out from the impurity along 45° diagonals.

Below we argue that the results consistent with the experiment on optimally doped samples require a value of U close to the threshold for the creation of static impurity-induced zero-field magnetism (i.e., close to the phase boundary in Fig. 2). This means that the field dependence can acquire nonlinearities, as shown in Fig. 6. For most of this work, we examine $U=1.75$, although we also exhibit the consequences of choosing other values.

The size of t assumed in order to compare with the experiment is probably a factor of 2–4 smaller than that deduced from angle-resolved photoemission spectroscopy (ARPES) experiments on cuprates, but we do not expect this to alter our qualitative conclusions. The low value of t is chosen such that reasonably low temperatures T/T_c can be accessed without encountering finite-size effects. For this choice, together with the choice of pair interaction V, $T_c=0.15$ corresponds to about 175 K, and the field parameter of $g\mu B/2=0.004$ corresponds to the experimental value of 7 T. The reader should therefore take the scales given in Kelvin only as extremely rough comparisons.

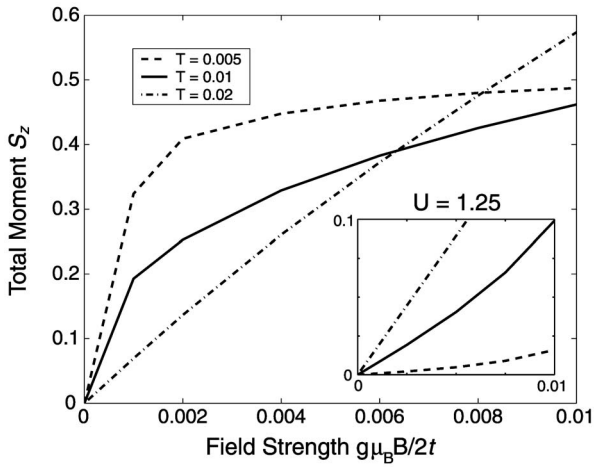

FIG. 6. The response S_z induced by a field B of a system with $U=1.75$ for three values of T. In the limit of zero field, the system is nonmagnetic regardless of temperature. Inset: field response for $U=1.25$.

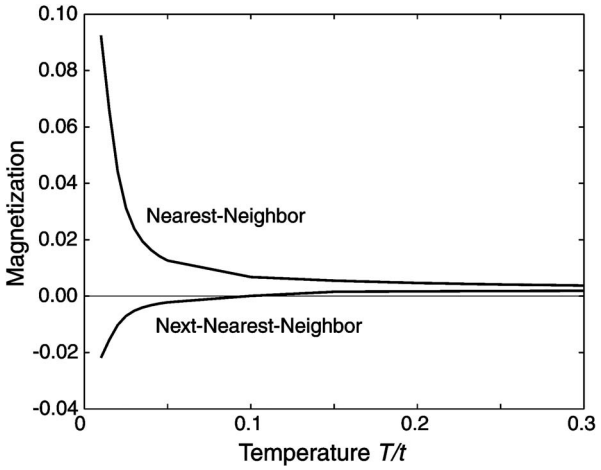

FIG. 7. Magnetization in fixed field $g\mu_B B/2=0.004$ vs T on the nearest-neighbor and next-nearest-neighbor sites for a strong impurity with $U=1.75$.

In the linear field response regime (Fig. 6), our calculations should be very similar to those of Ohashi for the nearest-neighbor weak-field susceptibility.[26] Thus, it is not surprising that we also find a strong increase of the magnetization on the nearest-neighbor sites as the temperature is lowered. This increase is weak in the normal state, then slows slightly at the superconducting transition as the gap opens, as depicted in Fig. 7. As the temperature is lowered further, the resonant state in the d-wave superconductor forms (Fig. 4), driving the susceptibility to a large value, which, however, is expected to saturate at $T\to0$, as indicated in the figure. We are unable to calculate results accurately below a temperature $T\simeq D(a/L)^2$, where $D\approx8t$ is the bandwidth, because the thermal energy becomes of the order of the level spacing in the finite-size system. For the simulations reported here, the cutoff is of the order of $T_{\min}\sim0.01$. The next-nearest-neighbor susceptibility is also enhanced, but has the opposite sign because the correlations are antiferromagnetic.

It is worth noting that, in the presence of the nonzero external field, a modulated local magnetic state is present even in the absence of the antiferromagnetic correlations driven by U. This is the analog, in the d-wave superconducting state, of Friedel-like spin-density oscillations, which represent the response of the normal metal to a local perturbation. As such, the oscillations necessarily take place at an incommensurate wave vector $2k_F$, which is, however, close to $(\pi/a,\pi/a)$ because the system is close to half filling. Note that these $U=0$ magnetization oscillations, shown in Fig. 8, are driven by the Pauli susceptibility in the d-wave superconductor. For a weak impurity, this response is quite weak at low temperatures, due to the linear ω dependence of the d-wave density of states near the Fermi level. On the other hand, the LDOS resonance at the Fermi level in the case of a strong impurity enhances this local response substantially. Note that the magnetization is always positive, however, since the local susceptibility is proportional to an enhanced LDOS at the Fermi level. When correlations are added, as indicated by the increasing U in Fig. 8, the response can be

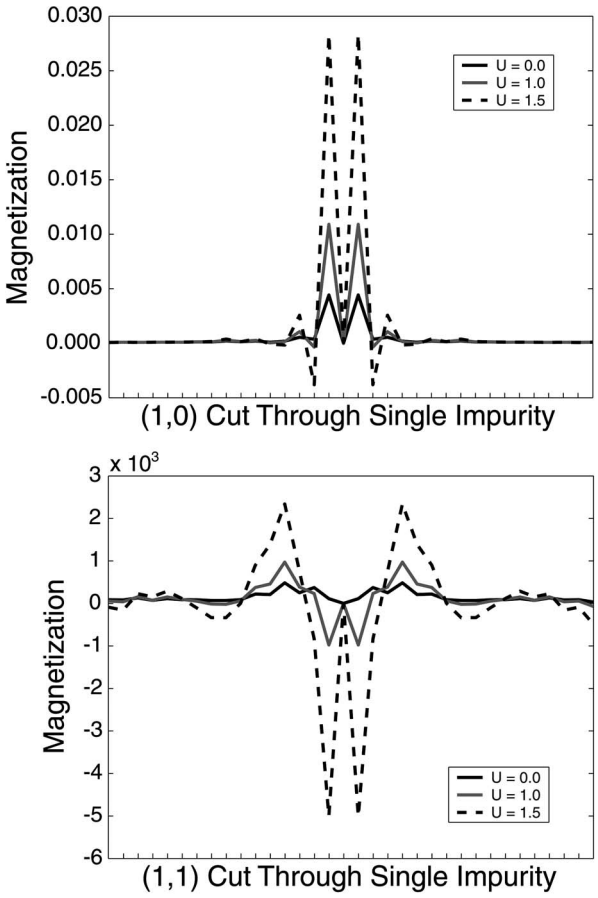

FIG. 8. Top: magnetization along (1,0) direction through impurity with on-site potential $V_{\mathrm{imp}}=100$, $g\mu_B B/2=0.004$, $U=0,1,1.5$, and $T=0.013$. Bottom: same but along the (1,1) direction.

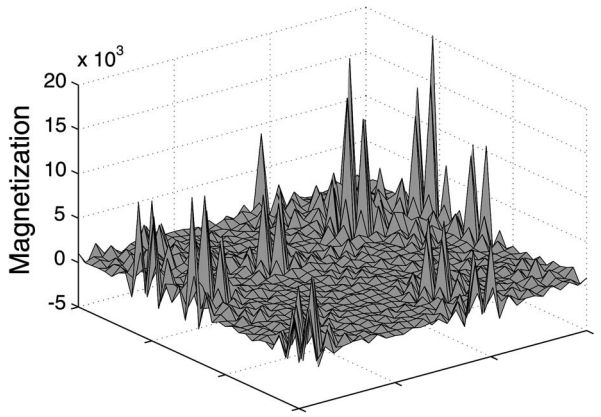

FIG. 9. Magnetization m for one configuration of a system with 1.5% random impurities and $U=1.25$, $T=0.013$, and $B=0.004$.

many times that of the pure BCS system with noninteracting quasiparticles, and it takes on an alternating character, as seen. These effects will lead to asymmetries in NMR line shapes, as discussed below. We note further that the "background" homogeneous magnetization of the system in nonzero external field is present in Fig. 8, but it is barely visible due to the small value of the homogeneous d-wave susceptibility at low T.

III. MANY-IMPURITY MAGNETIZATION

In the presence of many strong impurities, the wave functions of electrons bound to the impurity interfere at long distances, leading to collective behavior which is no longer describable by the one-impurity model. These effects have been studied in d-wave superconductors without antiferromagnetic correlations.[27–33] The interference of the many-impurity states leads to a splitting of bound state energies and an accumulation of low-energy impurity-induced energy eigenvalues, which are spread out over a so-called "impurity band." In the d-wave case, the formation of the impurity band and the corresponding quasiparticle localization problem are strongly influenced by the fact that significant overlaps between two impurity states can take place only if the impurities are "oriented" with respect to one another such that the nodal quasiparticle wave functions overlap along the [110] direction. In fact, analysis of the two-impurity problem shows that interference effects can take place over many tens of lattice spacings between optimally oriented impurities.[29–31] In systems with percent level disorder, however, these effects are also significant for pairs of impurities aligned along the [100] direction.

In the presence of correlations, interference effects extend to the magnetic channel and are enhanced by increasing U. In Fig. 9, we show a system in applied field in the presence of many strong impurities. It is clear that the size of the magnetization on nearest-neighbor sites varies significantly according to the local disorder environment. To clarify this, we compare a few of these impurities in the many-impurity sample with the comparable impurity in isolation in Fig. 10.

The distribution of magnetizations shown in Fig. 9 represents all the information necessary to calculate the NMR response within our approach, since it determines the distribution of nuclear-spin precession frequencies, in different linear combinations depending on the locations of the nuclei relative to the Cu sites. We focus in more detail on the actual NMR lines in Secs. IV and V below. For now, we are interested in showing how interference effects influence the "bare" distribution of magnetizations. To this end, we collect all the magnetizations in the system in a histogram for a single impurity, then compare to progressively larger impurity concentrations in Fig. 11. For a single impurity, small satellite peaks are visible in the spectrum since the same magnetization value appears on all sites with fourfold symmetry. Note that the satellite peaks associated with the nearest-neighbor sites occur at magnetization values well outside the range of the plot. With the addition of a few random impurities, these magnetization values are split, the distribution is smeared, and satellites are seen to disappear already at subpercent level concentrations. In addition, positive magnetizations are seen to be preferentially enhanced due to the density of states effects discussed above.

It is interesting to ask why interference effects in the magnetic channel are so important in the superconducting state that satellite features are immediately eliminated. To this end, we plot the distribution of magnetization values in real space in Fig. 12. It is seen that those values which contribute

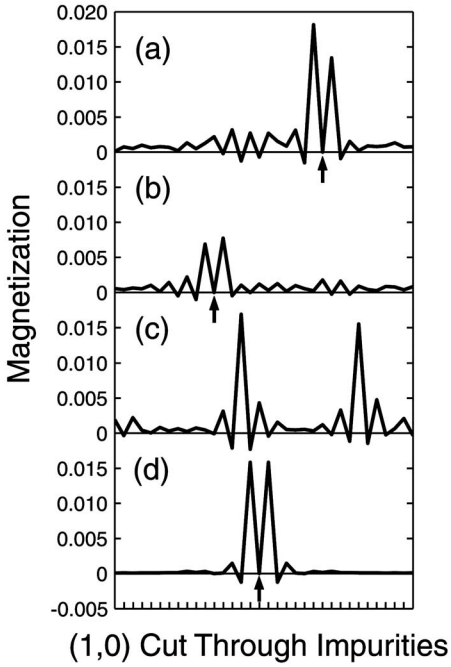

FIG. 10. [(a)–(c)] 0° magnetization cuts through 1% impurity systems and (d) a single isolated impurity, taking $U=1.25$, $T=0.013$, and $g\mu_B B/2=0.004$. The arrows indicate a cut passes through an impurity site, where magnetization is zero, and large peaks occur on nearest-neighbor sites. Interference effects can both enhance and suppress nearest-neighbor magnetizations relative to the one-impurity result shown at the bottom. Note that the cut in panel (c) does not pass through an impurity site but passes through two nearest-neighbor sites.

to the satellites close to the peak (which eventually determine the width of the line for a finite density of scatterers) are primarily located in the 45° tails of the quasiparticle wave functions some 10–15 lattice spacings from the impurity site (see below, however). The orbital parts of these

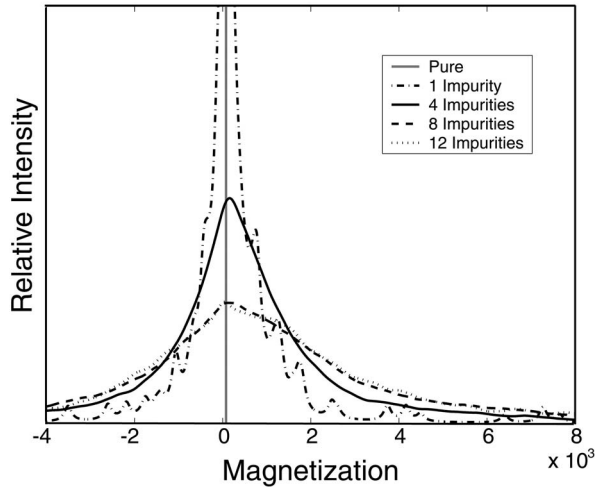

FIG. 11. Magnetization histogram for a 34×34 system with $U=1.75$ and 1, 4, 8, and 12 impurities at $T=0.013$ and $g\mu_B B/2=0.004$.

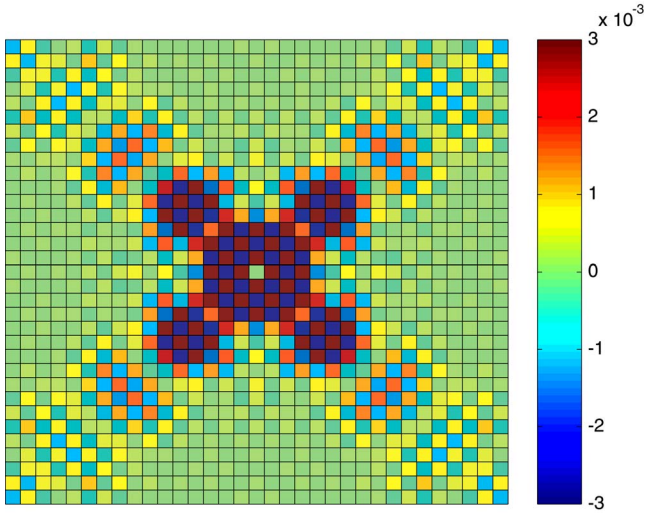

FIG. 12. (Color online) Distribution in real space of magnetization values around a single $V_{\mathrm{imp}}=100$ impurity with $U=1.75$, $T=0.013$, and $g\mu_B B/2=0.004$.

wave functions are known to strongly interfere in the absence of correlations, provided other impurities are appropriately oriented, so it is no great surprise that the magnetic parts of these wave functions also strongly interfere.

Any bulk measurement of magnetization results in an average over this smeared magnetization distribution. In addition, the temperature dependence of the magnetization depends on their position relative to the impurity. Contributions from sites far from impurities decrease with decreasing temperature, as for the homogeneous d-wave superconductor. Impurity nearest-neighbor susceptibilities are strongly enhanced, in the other hand. These effects combine to determine the total temperature dependence of thermodynamic properties. For example, if one measures the total susceptibility of the sample, it exhibits an upturn at low T if the density of impurities is a significant fraction of the sample (Fig. 13).

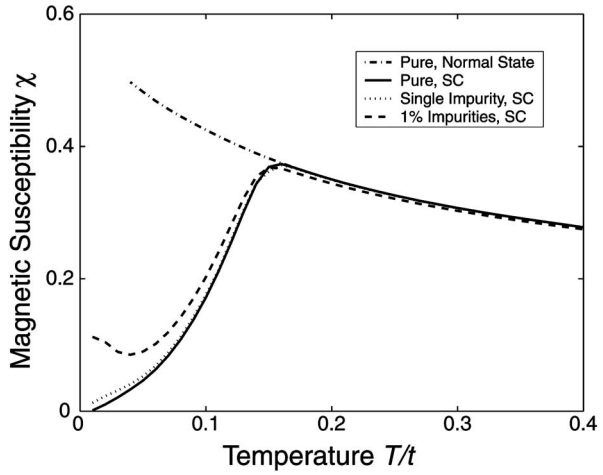

FIG. 13. Magnetic susceptibility per site $(1/L^2)dS_z/dB$ for a 28×28 system at $U=1.25$ for normal state ($d=0$), superconducting state, one impurity, and 1% impurities.

IV. IMPURITY CONTRIBUTION TO ^{17}O LINE

A. Disorder dependence of ^{17}O line

The planar ^{17}O nucleus is situated halfway between two Cu sites or between a Cu and a Zn. It is assumed that it senses the local field proportional to the sum of the magnetizations on the two sites closest to it. For example, O nuclei far from the impurities are subjected to $2\chi_{\rm hom}B$, where $\chi_{\rm hom}$ is the susceptibility of the homogeneous system, whereas an O nucleus next to a Zn atom is subjected to $(\chi_{nn}+0)B$, since there is effectively zero electron density on the Zn site by assumption. Nuclei at varying distance from the impurity will measure different combinations of local magnetizations.

In an NMR experiment, the resonance frequency ν of a nucleus is given by

$$\nu = \frac{\gamma}{2\pi} B(1 + K_{\rm orb} + K_{\rm spin}), \tag{11}$$

where γ is the gyromagnetic ratio of the nucleus, B is the applied magnetic field, $K_{\rm orb}$ is the T-independent orbital contribution of valence and inner-shell electrons, and $K_{\rm spin}$ is the spin contribution from the electrons. In a simple metal or in a cuprate above T_c, $K_{\rm spin}$ is proportional to the uniform electronic spin susceptibility $\chi_{\rm spin}$ through

$$K_{\rm spin} = \frac{A_{hf}\chi_{\rm spin}}{\mu_B}, \tag{12}$$

where A_{hf} is the hyperfine coupling between the nucleus and the electrons and μ_B is the Bohr magneton. In the specific case of ^{17}O NMR for planar oxygens, a ^{17}O nucleus at position $(x;y)$ is coupled to the spin susceptibility through its two neighboring Cu, leading to[34]

$$^{17}K_{\rm spin}(x,y) = \frac{^{17}A_{hf}\left[\chi_{\rm spin}\left(x+\frac{1}{2};y\right)+\chi_{\rm spin}\left(x-\frac{1}{2};y\right)\right]}{\mu_B}, \tag{13}$$

where we assumed here an oxygen lying along the x axis, with x and y the Cu coordinates in units of the Cu lattice spacing a.

In the pure metallic state above T_c, $\chi_{\rm spin}$ is uniform, so that the NMR consists of a single line shifted by $^{17}K_{\rm spin}=2\,^{17}A_{hf}\chi_{\rm spin}/\mu_B$. In the superconducting state, the situation is more complex because of the presence of the vortex lattice. Equation (13) stays valid, but $B(\mathbf{r})$ is no longer uniform. As the NMR spectrum is a histogram of all the frequencies $\nu(\mathbf{r})$, this spectrum directly reflects the vortex field distribution, assuming that orbital and spin shifts stay uniform (see, for example, Ref. 35).

Let us now consider how the impurities affect the NMR spectrum. If an impurity induces a spatially dependent magnetization as computed above, it can be regarded as a distribution of the susceptibility $\chi_{spin}(x;y)$ among Cu sites, leading to a distribution of K_{spin}, i.e., a broadening of the NMR spectrum. When both impurities and superconductivity are now taken into account, the NMR spectrum should be distributed simultaneously by a distribution of the local field $B(\mathbf{r})$ due to the vortex lattice and by a distribution of spin shifts $K_{spin}(\mathbf{r})$ due to the impurities. However, these two distributions are uncorrelated, as argued in Ref. 9. They should then simply convolve with each other.

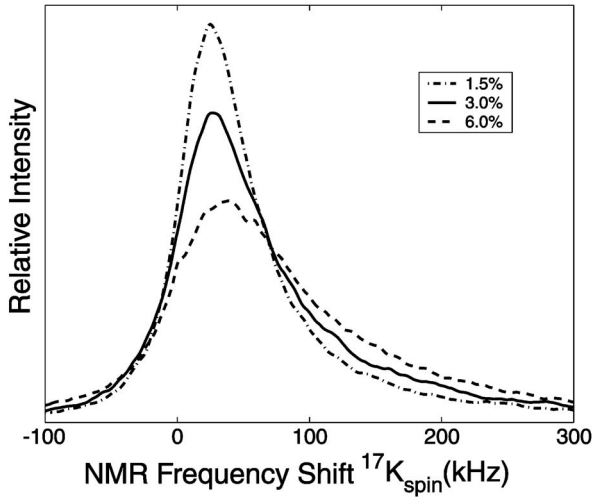

FIG. 14. ^{17}O NMR shift calculated from Eq. (13) for $U=1.75$ for a 34×34 system averaged over 15 random impurity configurations at $g\mu_B B/2=0.004$ and $T=0.013$. Numerical smoothing was performed by convolving the distribution with a Lorentzian width of 3.5 kHz.

In Fig. 14, we show how the distribution of magnetizations is transformed into a distribution of ^{17}O frequency shifts due to disorder alone. As expected, increasing disorder broadens the line. In addition, however, it is seen that the line asymmetry increases, with enhanced weight on the positive side. This effect was indeed observed in experiment, and attributed to the enhanced spin susceptibility, i.e., density of states near the Fermi level due to impurities. Thus, some small line asymmetry would result simply because the density of states of a disordered d-wave superconductor is enhanced in the interstitial regions far from the impurity, but as we have seen, the susceptibility is also enhanced due to correlation effects, which are also affected by interference of many impurities.

In order to compare our computation to the experimental NMR lines in the presence of Zn below T_c, we must now estimate the effects of the vortex lattice. The idea is to produce a series of NMR lines corresponding to the pure system in the presence of the vortex lattice field modulation, renormalized by the disorder-enhanced magnetic penetration depth for each impurity concentration. These lines include, in principle, the effects of spatially varying superflow but not of spatially varying spin magnetization.

Simulating the vortex field distribution including quasiparticle contributions with high accuracy is probably difficult even in the nominally pure case due to uncertainties regarding the origin and statistical nature of the disorder in the vortex lattice. Following Ref. 9, we therefore identify empirically the vortex-induced part of the field distribution in the superconducting state with the field-independent part of the overall NMR shift. We accept the determination of the width and shift of the field-independent part of the distribu-

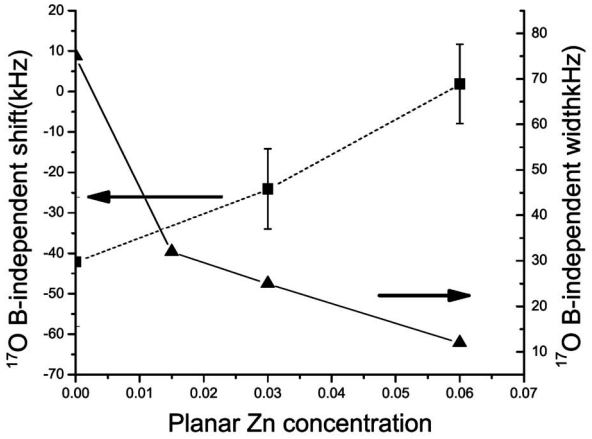

FIG. 15. Field-independent experimental ^{17}O shifts (squares) and widths (triangles) from Ref. 9. Note no field-independent shift was determined for the 1.5% sample.

tion determined by Ouazi *et al.*,[9] shown in Fig. 15, and estimate the vortex contribution by the Lorentzians determined using these parameters. The lines thus obtained are shown in Fig. 16. Note that the data for the 1.5% Zn sample were not good enough to extract the field-independent part; we have therefore simply interpolated linearly between the pure and 3% sample.

These lines are now convolved with the distributions of ^{17}O NMR shifts obtained from the impurity effects alone. This is justified because in fields of a few tesla the intervortex distance is of the order of hundreds angstroms, whereas the typical interimpurity distance for samples with percent level Zn is tens angstroms. Thus, there can be no significant correlation between the positions of most of the Zn atoms and the vortices themselves.

To obtain the corresponding ^{17}O shifts, we now use the values $\gamma/2\pi=5.772$ MHz/T, $^{17}A_{hf}=36$ kOe (Refs. 36 and 37) and $^{17}K_{\mathrm{orb}}=0.02\%$,[34] which apply for the external field along the c crystallographic axis, as in Ref. 9. Finally, we convolve both the impurity and vortex field distributions. The lines thus obtained are plotted in Fig. 17 and compared to the experimental results of Ouazi *et al.*[9] taken at 15 K. The semiquantitative variation of the width and asymmetry

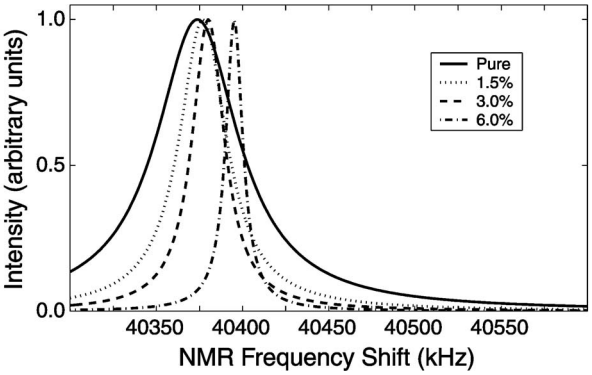

FIG. 16. Lorentzian vortex field distributions deduced from field-independent data of Ouazi *et al.* (Ref. 9). Note the 1.5% curve was obtained by interpolating the shift of the 1.5% sample.

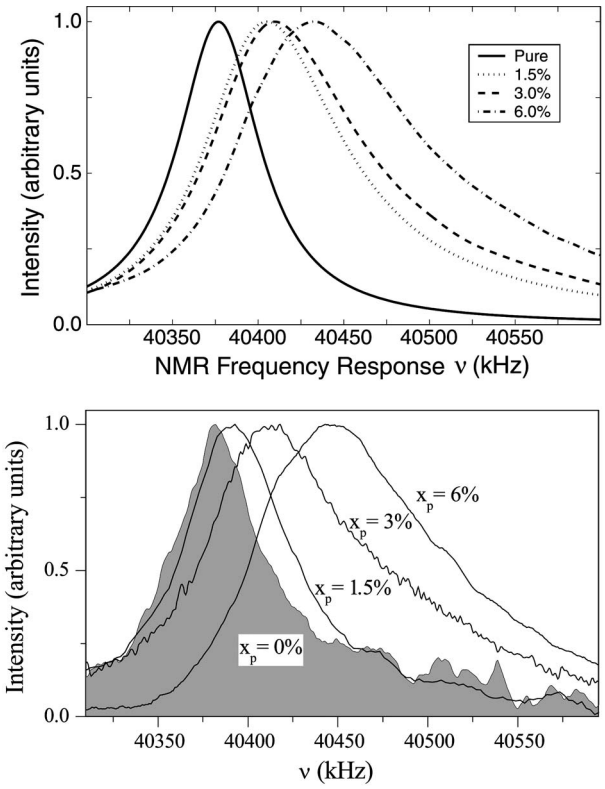

FIG. 17. Top: normalized theoretical ^{17}O NMR lines at $T=0.013$ and $g\mu_B B/2=0.004$ obtained by the procedure described in the text, for $U=1.75$ and planar Zn concentrations of $x_p=0\%, 1.5\%, 3\%$, and 6%. Bottom: experimental results on YBCO powders from Ref. 9 for the same concentrations in a 7 T field at 15 K.

of the experimental lines with impurity concentration are seen to be remarkably well reproduced by the theoretical results. In addition, the magnitudes of the shifts for different Zn concentrations are quite well reproduced, with the exception of the 1.5% sample, where the shift of the vortex field distribution was effectively unknown. We note that no extensive fitting in parameter space was done, so it is quite striking that the magnitudes and dependence on concentration agree so quantitatively.

To make further quantitative comparisons with the widths, which are the more experimentally reliable quantities, we plot in Fig. 18 the same normalized lines shown in Fig. 17, but with the shifts removed. It is seen that the theory tracks the increase in width as well as the overall line shape extremely well.

B. *T* dependence of line asymmetry

Ouazi *et al.*[9] observed an increase in the NMR line *asymmetry*, with a shift in weight toward the positive side, as Zn concentration was increased and/or as the temperature was lowered. They proposed that this phenomenon was associated with the formation of the resonant state around Zn observed by STM, increasing the LDOS at the Fermi level near the impurity, and thereby enhancing the spin susceptibility. Since the LDOS enhancement is always positive, this effect

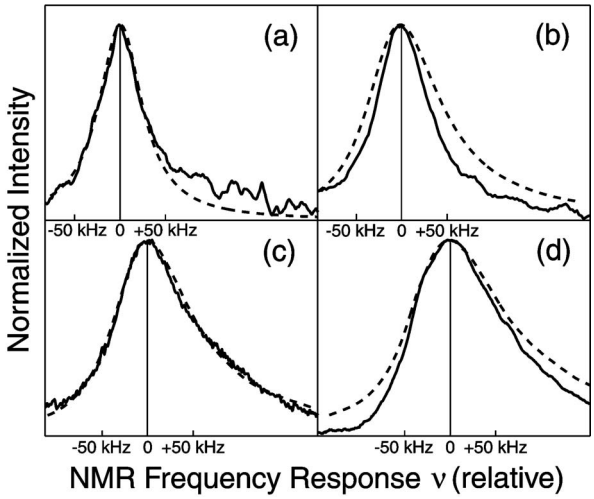

FIG. 18. Normalized experimental ^{17}O NMR lines of Ref. 9 at 15 K and 7 T with all shifts removed (solid lines) and normalized theoretical impurity NMR lines for $U=1.75$ convolved with vortex field distributions as described in the text; shifts also removed (dashed lines): (a) pure, (b) $x_p=1.5\%$, (c) $x_p=3.0\%$, and (d) $x_p=6.0\%$.

selectively enhances the broadening on the positive side of the line, provided it exceeds in magnitude the homogeneous magnetization in the regions of the sample far from impurities. In a *d*-wave superconductor, this is always true at sufficiently low T since the bare susceptibility of the clean system vanishes as $\sim T$ at low temperatures. Note that this LDOS-based asymmetry enhancement is essentially the same effect to which the LDOS-only approaches mentioned above ascribe the entire enhancement of the local susceptibility measured in NMR. We have already argued that this is a small effect with regard to the overall T dependence in the near field of the impurity; here, we show that it can nevertheless play an important role in the T-dependent structure of the line, and in particular the asymmetry of the linewidth, which arises from contributions further from the impurities.

We find that the explanation given by Ouazi *et al.*[9] is essentially correct, but is strongly enhanced both by interference between multiple impurities and by antiferromagnetic correlations. We have seen that the susceptibility on the sites nearest the impurity is strongly increased as the temperature is lowered (Fig. 7) and that this effect is magnified by increasing U (Fig. 8). The enhancement of the asymmetry of the line shape due to the interference effect for fixed temperature was mentioned above and illustrated in Fig. 14. We therefore anticipate that the low-T upturns in the asymmetry of the line shape will be a characteristic of the present model as well.

To see the origin of the asymmetry enhancement at low T, let us first examine the temperature dependence of the magnetization of those sites which actually determine the measured width. This is not a completely straightforward proposition, given that the magnetization patterns in the *d*-wave superconducting state are determined by a combination of normal Friedel oscillations, local magnetic correlations, *d*-wave pair correlations, and interference in the many-impurity case. Even for a single impurity, the first three effects combine to make it difficult to specify, e.g., a given distance from the impurity which is important in determining the linewidth. It is clear that it is not the nearest-or next-nearest-neighbors which do so, but as shown in Fig. 19, the set of sites actually contributing to the positive and negative half-widths—while indeed clustered around a range of 10–15 lattice spacings from the impurity in the nodal tails of the wave functions, as noted above—form a more complicated pattern.

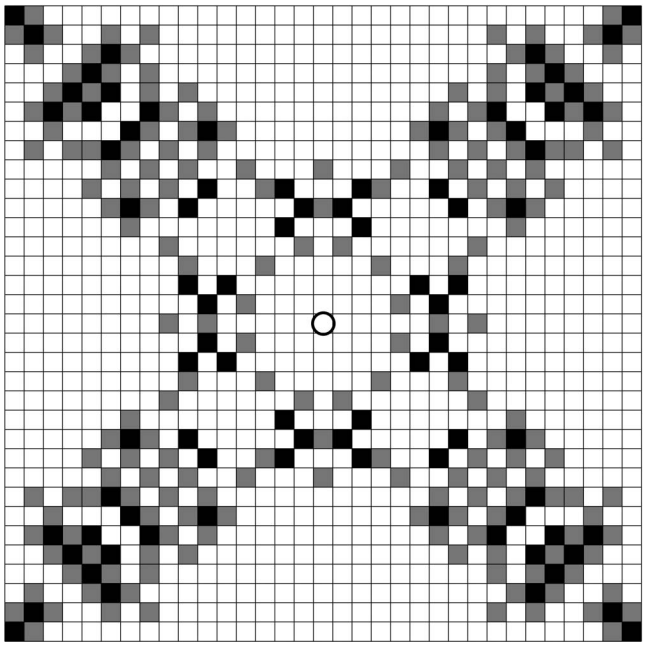

FIG. 19. Single impurity of strength $V_{\mathrm{imp}}=100$ indicated by circle at center of 34×34 system. Sites with magnetization values within ranges such as to determine NMR linewidth for $U=1.75$, $T=0.01$, and $g\mu_B B/2=0.004$. Sites with $-0.0015\leqslant m\leqslant-0.0001$ ("ν_L sites") are colored black, and those with $0.0005\leqslant m\leqslant0.002$ ("ν_H sites") are colored gray.

The temperature dependence of these selected sites is now shown in Fig. 20, where the influence of electronic correlations is also illustrated by comparing $U=1.75$ and $U=0$. In the noninteracting case, we can see the low-temperature upturn of the nearest-neighbor magnetization, as discussed in Ref. 12 (note that at $T\rightarrow0$, the noninteracting local susceptibility always $\rightarrow0$ since the impurity resonance sits at a finite energy for any generic potential). On the other hand, the upturn of the magnetization of the sites contributing to the linewidth is much weaker to nonexistent in the noninteracting case, although the LDOS effect still manifests itself via the fact that $\Delta\nu_L<\Delta\nu_H$. In the $U>0$ case, however, the upturns are much stronger, and even manifest the saturation of the magnetization arising from $\Delta\nu_L$ sites observed in experiment,[9] which leads to the surprising increase of the $\Delta\nu_H-\Delta\nu_L$ observed.

To verify if the phenomenon is reproduced quantitatively, we plot explicitly the difference of the half-width at half maximum on the high frequency side of the ^{17}O line, $\Delta\nu_H$, and the same quantity on the lower side $\Delta\nu_L$. Each is independently enhanced at low temperatures, but it is the difference which is particularly striking, as seen in Fig. 21, where

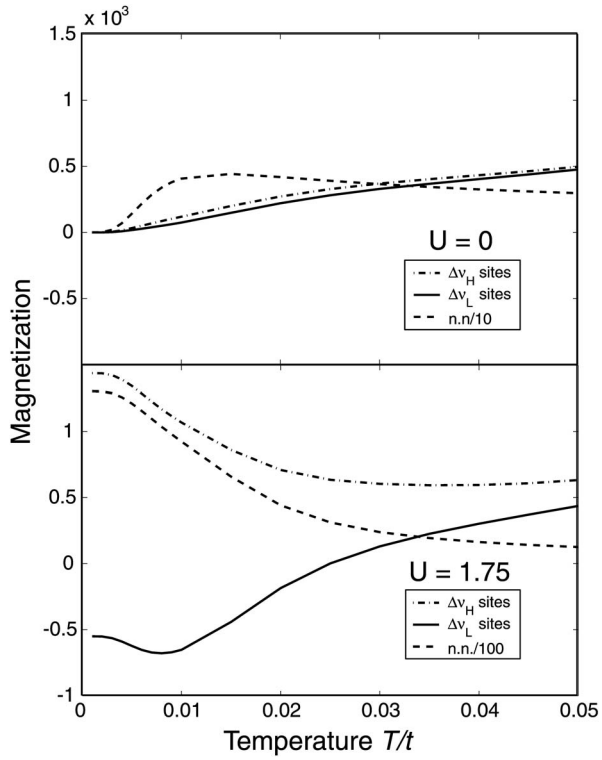

FIG. 20. Temperature dependence of magnetization on sites identified as contributing to determination of NMR linewidth, as specified in Fig. 19.

the theory for $U=1.75$ is compared with the results of Ouazi *et al.*[9] shown in Fig. 22. While the details of the theoretical curves do not agree exactly with experiment, it is clear that the basic results are reproduced by the theory, both in terms of the temperatures at which the upturns begin and in terms of the magnitudes of the upturns themselves. On the other hand, the lower half-width $\Delta\nu_L$ is roughly T independent in experiment, but it has a weaker but still significant enhancement in the calculation, as indicated in Fig. 19. We do not understand the origin of this discrepancy at present. In addition, the theoretical result retains a certain asymmetry of the line shape up to higher temperatures, whereas the experimental line shape becomes symmetric above about 40 K. This may be due to the neglect of inelastic scattering, which becomes important at higher T, in the calculation.

The two figures shown in Fig. 21 correspond to two different values of the impurity potential V_{imp}. The upper panel corresponds to a value $V_{\text{imp}}=100$, which gives an impurity resonance energy of $\Omega_0 \simeq -0.01$, whereas the $V_{\text{imp}}=10$ lower panel corresponds to a resonance energy of $\Omega_0 \simeq 0$ within our numerical resolution, for this particular band. Thus, the local Fermi level density of states near the impurity is larger in the second case, leading indeed to a stronger upturn, as anticipated. The actual resonance energy of a Zn in YBCO is unknown at this time, but is expected to be close to the −1.5 meV observed in BSCCO-2212.

V. FURTHER COMPARISONS WITH EXPERIMENT: ^{7}Li

The "universality" of the magnetic response to strong in-plane *nonmagnetic* defects was noted early on by Bobroff

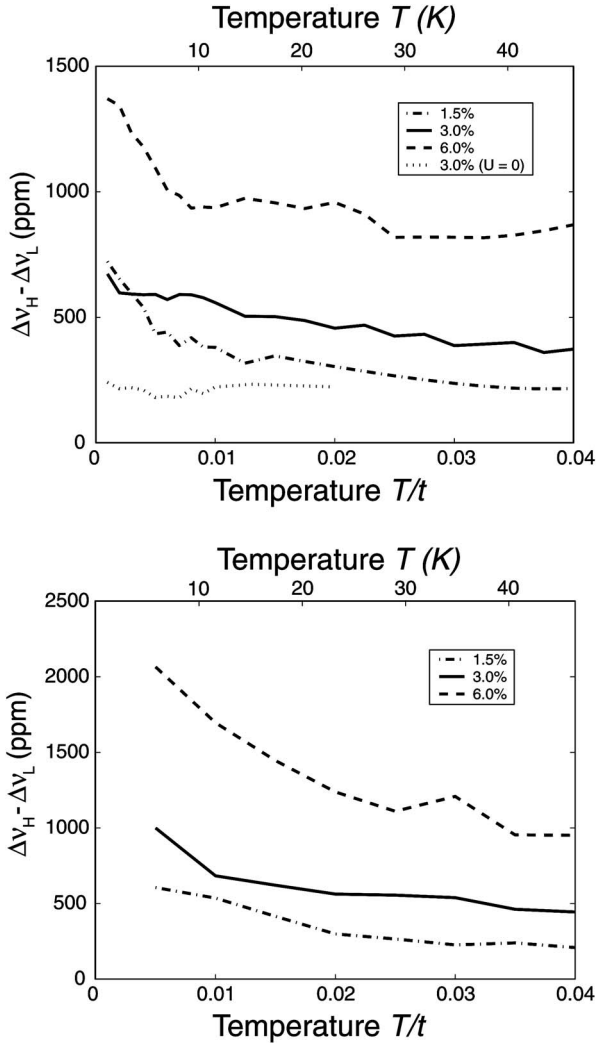

FIG. 21. Line asymmetry—theory: difference of half-widths on negative ($\Delta\nu_L$) and positive ($\Delta\nu_H$) frequency sides of NMR lines vs T for five impurity concentrations. Top panel: $U=1.75$, $g\mu_B B/2=0.004$, and $V_{\text{imp}}=100$. The result for $U=0$ is also shown for comparison (dotted line). Bottom panel: same, but with $V_{\text{imp}}=10$.

et al.[3] That is, any in-plane impurity which from a conventional chemistry standpoint is expected to be nonmagnetic appears to have a nearly identical effect on both normal state and superconducting properties. This includes Zn, Li, and defects in the plane created by electron irradiation, which produce nearly identical changes in susceptibility T_c and resistivity per in-plane impurity. This is remarkable because there would appear to be important electronic structure differences between the Zn ion, which has a closed shell, and Li, which is believed to localize a hole around itself. It is generally believed that the essential features of these defects are therefore simply their ability to exclude mobile conduction electrons, hence our choice of model of, e.g., Zn as a strong repulsive potential. Within this assumption of universality of in-plane nonmagnetic defects, we can take the results for the magnetization distribution in the disordered system already produced, and use them to describe the results of earlier ^{7}Li NMR experiments on YBCO.

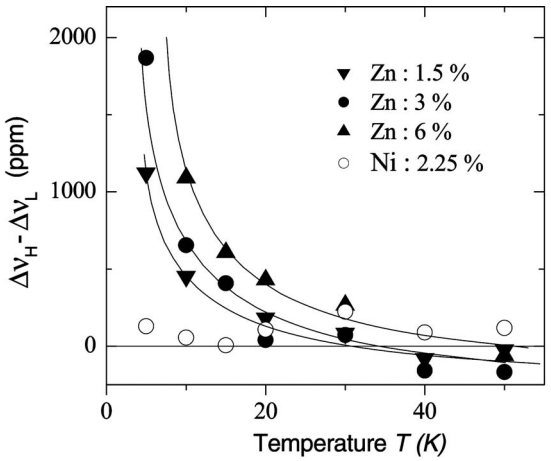

FIG. 22. Line asymmetry—experiment: difference of half-widths on negative ($\Delta\nu_L$) and positive ($\Delta\nu_H$) frequency sides of NMR lines vs T for three Zn concentrations (from Ref. 9).

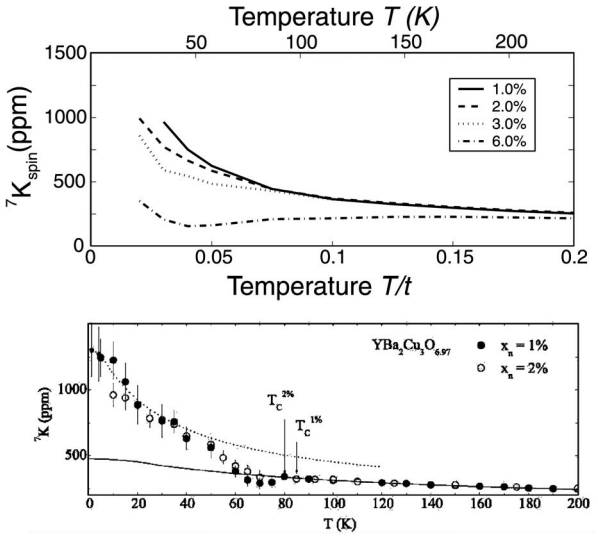

FIG. 23. Upper panel: Li Knight shift as calculated in the text, using the same magnetizations, obtained for same parameters as shown in the histograms in Fig. 11 with three random configurations. Lower panel: experimental Knight shift data from Ref. 8 for $x_p=1\%$ and 2% Li in optimally doped YBCO for $B=7$ T. The dashed and solid lines are fits to local susceptibility of Kondo model at low and high temperatures, respectively.

Li has the thus far unique ability in the cuprates to simultaneously provide an in-plane impurity and a nucleus (^{7}Li) suitable for NMR. The signal is therefore not complicated by contributions from regions of the sample far from impurity sites, but provides direct information about the immediate vicinity of the impurity, which replaces a Cu in the CuO_2 plane. We will assume, as in prior work, that the Li provides a shift equal to the sum of the magnetizations on its nearest-neighbor sites, leading to a shift [compare Eq. (13)].

$$^7K_{\rm spin}(\mathbf{r}) = \frac{^7A_{hf}\sum_{\delta}\chi_{\rm spin}(\mathbf{r}+\delta)}{\mu_B}, \tag{14}$$

where δ is a nearest-neighbor displacement. The results plotted as a function of temperature are shown in Fig. 23 and compared to the experimental results on Li substituted in optimally doped YBCO of Bobroff *et al.*[8] The theory seems to reproduce the initial weak dependence on the Li concentration (nonexistent in the normal state, small in the superconducting state). This is because the Li impurities are sensitive to their local environment only, and the shift does not therefore depend on concentration until interference effects become significant. Until now, experiments have only been performed on a maximum of 2% planar Li impurities; the deviations of the curves corresponding to higher concentrations at low temperatures constitute predictions of the theory which can be verified by NMR. We note that the experimental results, in particular the change in slope near T_c and the subsequent rise at low T, have been discussed in terms of the effect of the opening of the superconducting gap on Kondo screening of simple moments by the d-wave quasiparticle gas.[38] Here, our results, which do not account for the spin-flip scattering necessary for the Kondo effect to take place at all, indicate that a strong-correlation explanation for these, and associated phenomena, is more likely.

VI. CONCLUSIONS

We have shown that a theoretical model of strong impurities in a d-wave superconductor, with residual quasiparticle interactions treated in a weak-coupling Hubbard model within a mean-field approximation, provides an excellent description of NMR experiments on optimally doped YBCO. This model assumes that both Zn and Li impurities act as simple strong potential scatterers which induce staggered magnetic polarization clouds around themselves with very small total moment *proportional to the external magnetic field*. The results and comparison with experiments on optimally doped YBCO are *not* compatible with static impurity-induced magnetism present in zero field. This is consistent with the lack of a magnetic μSR signal over most of the YBCO phase diagram down to very low doping,[19] and with the absence of a Schottky anomaly in specific heat measurements.[39] The universal response of the system to nonmagnetic defects, which are very different chemically, also confirms the primacy of the strong correlations in the CuO_2 plane for these phenomena.

The ability of NMR to probe nuclei with different configurations with respect to the Cu spins means that different interesting aspects of the physics can be tested by the model. In particular, the ^{17}O line is primarily a probe of the weaker magnetism induced far from the impurities. It is thus more sensitive to the effects of interference of the quasiparticle bound states associated with different scattering centers. We have shown that this quasiparticle interference is responsible for the enhancement of the ^{17}O linewidth as measured by experiment, and the variation of this line shape with Zn concentration has been quantitatively reproduced by the model. The low-temperature enhancement of the ^{17}O line to the positive side caused by Zn appears, within this framework, to be related to the LDOS enhancement around the impurities, as suggested by Ouazi *et al.*[9] On the other hand, the size and strong temperature dependences of the line broadening can be understood only if electronic correlations and concomitant paramagnetic local moments are present.

The ^{7}Li nucleus, which senses only the nearest-neighbor Cu, gives us a picture into magnetic effects in the vicinity of the individual impurities. Our study, which quantitatively reproduces the ^{7}Li Knight shift magnitude and T dependence in both the normal and superconducting states, concludes that experiments on Li done thus far have probed only the regime of individual isolated impurities, where interference effects are not strong enough to affect the nearest-neighbor sites, but these should be visible by going to only slightly higher Li concentrations. In addition, it shows how resonant states in the d-wave superconductor enhance both the single-impurity magnetic effects and the quasiparticle interference.

We note a number of questions which are open and which should be clarified in subsequent work. First, the current framework is a weak-coupling mean-field approach which neglects the renormalization of the electronic structure near the impurity sites found in strong-coupling approaches. We anticipate that such effects, which arise from diagrams not included in the randon phase approximation (RPA)-type analysis here, will give rise to quantitative changes in the values of parameters chosen here to fit the experiment, but they will not alter the overall physical picture we have presented. Many of these issues have already been raised and understood in the context of homogeneous RPA-level spin-fluctuation theories, where a reduced effective interaction U replaces the bare U after resummation of a subclass of diagrams. It is intriguing to note that NMR experiments seem to require us to work very close to the magnetic phase transition in the theory in order to explain, e.g., the magnitude of the linewidth and the T dependence of the line asymmetries. This is reminiscent of the early fits of spin-fluctuation theories of NMR for the homogeneous systems, which required values of the effective interaction to be close to the bulk transition in the model. Taken together, it is tempting to speculate that these results indicate the flow of the true Hamiltonian of the system to strong coupling at sufficiently low energies.

In this work, we have not carefully investigated the transition to the normal state, which we reserve for a subsequent paper. It is interesting to note that, while earlier works on the normal state using the same model[5,6] found it necessary to introduce an extended impurity potential to fit experiment, our conclusion is that this is not necessary in the superconducting state. Following Bulut's suggestion[40] that the extended nature of scattering potential may arise in the normal state from the renormalization of the local electronic structure by correlations, this may be an indication that the processes leading to this effect are simply gapped below T_c.

Finally, we emphasize that our calculation does not include spin-flip scattering terms necessary to recover a true Kondo effect and that, to the extent our analysis has been successful, our results therefore imply that Kondo physics is probably unnecessary to describe the phenomena in question, at least at optimal doping. It will be interesting to see whether the phenomenology put forward here continues to hold as one goes to underdoped systems with planar impurities which remain paramagnetic. Other possible extensions include more strongly interacting and/or more disordered systems, where static magnetism in zero field may be present, studies of the normal state, as well as of the overdoped regime. Work along these lines is in progress.

ACKNOWLEDGMENTS

The authors acknowledge stimulating conversations with H. Alloul and T. Nunner. Partial support for this research (B.M.A. and P.J.H.) was provided by ONR N00014-04-0060, DOE DE-FG02-05ER46236, and by a visiting scholar grant from CNRS (P.J.H.).

[1] A. M. Finkelstein, V. E. Kataev, E. F. Kukovitskii, and G. B. Teitelbaum, Physica C **168**, 370 (1990).
[2] A. V. Mahajan, H. Alloul, G. Collin, and J. F. Marucco, Phys. Rev. Lett. **72**, 3100 (1994).
[3] J. Bobroff, W. A. MacFarlane, H. Alloul, P. Mendels, N. Blanchard, G. Collin, and J.-F. Marucco, Phys. Rev. Lett. **83**, 4381 (1999).
[4] N. Bulut, Phys. Rev. B **61**, 9051 (2000).
[5] N. Bulut, Physica C **363**, 260 (2001).
[6] Y. Ohashi, J. Phys. Soc. Jpn. **70**, 2054 (2001).
[7] Y. Ohashi, Phys. Rev. B **66**, 054522 (2002).
[8] J. Bobroff, H. Alloul, W. A. MacFarlane, P. Mendels, N. Blanchard, G. Collin, and J.-F. Marucco, Phys. Rev. Lett. **86**, 4116 (2001).
[9] S. Ouazi, J. Bobroff, H. Alloul, M. Le Tacon, N. Blanchard, G. Collin, M. H. Julien, M. Horvatić, and C. Berthier, Phys. Rev. Lett. **96**, 127005 (2006).
[10] G. V. M. Williams, J. L. Tallon, and R. Dupree, Phys. Rev. B **61**, 4319 (2000).
[11] S. H. Pan, E. W. Hudson, K. M. Lang, H. Eisaki, S. Uchida, and J. C. Davis, Nature (London) **403**, 746 (2000).
[12] J. Chang, Y. H. Su, H. G. Luo, H. T. Lu, and T. Xiang, Phys. Rev. B **70**, 212507 (2004).
[13] I. Martin, G. Ortiz, A. V. Balatsky, and A. R. Bishop, Int. J. Mod. Phys. B **14**, 3567 (2000); M. Ichioka, M. Takigawa, and K. Machida, J. Phys. Soc. Jpn. **70**, 33 (2001); Y. Chen, Z. D. Wang, J.-X. Zhu, and C. S. Ting, Phys. Rev. Lett. **89**, 217001 (2002); H.-Y. Chen and C. S. Ting, Phys. Rev. B **71**, 220510(R) (2005); B. M. Andersen, I. V. Bobkova, P. J. Hirschfeld, and Yu. S. Barash, *ibid.* **72**, 184510 (2006); Phys. Rev. Lett. **96**, 117005 (2006); M. Mayr, cond-mat/0604636 (to be published).
[14] Y. Chen and C. S. Ting, Phys. Rev. Lett. **92**, 077203 (2004).
[15] Z. Wang and P. A. Lee, Phys. Rev. Lett. **89**, 217002 (2002).
[16] H. Tsuchiura, Y. Tanaka, M. Ogata, and S. Kashiwaya, Phys. Rev. B **64**, 140501 (2001).
[17] For a recent review see A. V. Balatsky, I. Vekhter, and J.-X. Zhu, Rev. Mod. Phys. **78**, 373 (2006).
[18] B. M. Andersen, A. Melikyan, T. S. Nunner, and P. J. Hirschfeld, Phys. Rev. Lett. **96**, 097004 (2006).
[19] J. Sonier, J. H. Brewer, and R. F. Kiefl, Rev. Mod. Phys. **72**, 769 (2000).
[20] Y. Sidis, P. Bourges, B. Hennion, L. P. Regnault, R. Villeneuve,

G. Collin, and J. F. Marucco, Phys. Rev. B **53**, 6811 (1996); Y. Sidis, C. Ulrich, P. Bourges, C. Bernhard, C. Niedermayer, L. P. Regnault, N. H. Andersen, and B. Keimer, Phys. Rev. Lett. **86**, 4100 (2001).

[21] P. Mendels, H. Alloul, J. H. Brewer, G. D. Morris, T. L. Dutty, S. Johnston, E. J. Ansaldo, G. Collin, J. F. Marucco, Ch. Niedermayer, D. R. Noakes, and C. E. Stonach, Phys. Rev. B **49**, 10035 (1994); C. Bernhard, Ch. Niedermayer, T. Blasius, G. V. M. Williams, R. De Renzi, C. Bucci, and J. L. Tallon, *ibid.* **58**, R8937 (1998).

[22] B. Lake, H. M. Rønnow, N. B. Christensen, G. Aeppli, K. Lefmann, D. F. McMorrow, P. Vorderwisch, P. Smeibidl, N. Mangkorntong, T. Sasagawa, M. Nohara, H. Takagi, and T. E. Mason, Nature (London) **415**, 299 (2002).

[23] H. Kimura, M. Kofu, Y. Matsumoto, and K. Hirota, Phys. Rev. Lett. **91**, 067002 (2003).

[24] B. M. Andersen and P. J. Hirschfeld, cond-mat/0607682, Physica C(to be published).

[25] Hiroshi Kontani and Masanori Ohno, Phys. Rev. B **74**, 014406 (2006).

[26] The extended impurity potential considered in Ref. 7 appears, in fact, to be driving a spontaneous moment, according to our calculations. This is probably responsible for the divergent susceptibility found.

[27] A. V. Balatsky and M. I. Salkola, Phys. Rev. Lett. **76**, 2386 (1996).

[28] U. Micheluchi, F. Venturini, and A. Kampf, J. Phys. Chem. Solids **63**, 2283 (2002).

[29] D. K. Morr, J. Schmalian, R. Stern, and C. P. Slichter, Phys. Rev. B **58**, 11193 (1998).

[30] L. Zhu, W. A. Atkinson, and P. J. Hirschfeld, Phys. Rev. B **67**, 094508 (2003).

[31] B. M. Andersen and P. Hedegård, Phys. Rev. B **67**, 172505 (2003).

[32] W. A. Atkinson, P. J. Hirschfeld, and L. Zhu, Phys. Rev. B **68**, 054501 (2003).

[33] B. M. Andersen, Phys. Rev. B **68**, 094518 (2003).

[34] M. Takigawa, P. C. Hammel, R. H. Heffner, Z. Fisk, K. C. Ott, and J. D. Thompson, Phys. Rev. Lett. **63**, 1865 (1989).

[35] A. P. Reyes, X. P. Tang, H. N. Bachman, W. P. Halperin, J. A. Martindale, and P. C. Hammel, Phys. Rev. B **55**, R14737 (1997).

[36] Y. Yoshinari, H. Yasuoka, Y. Ueda, K. Koga, and K. Kosuge, J. Phys. Soc. Jpn. **59**, 3698 (1990).

[37] P. Butaud, M. Horvatić, Y. Berthier, P. Segransan, Y. Kitaoka, and H. Katayama-Yoshida, Physica C **166**, 301 (1990).

[38] C. R. Cassanello and E. Fradkin, Phys. Rev. B **53**, 15079 (1996).

[39] D. L. Sisson, S. G. Doettinger, A. Kapitulnik, R. Liang, D. A. Bonn, and W. N. Hardy, Phys. Rev. B **61**, 3604 (2000).

[40] N. Bulut, Phys. Rev. B **68**, 235103 (2003).